

The time-variable ultraviolet sky: Active Galactic Nuclei, Stars and White Dwarfs

R. Bühler¹ and J. Schliwinski²

¹ Deutsches Elektronen-Synchrotron DESY, Platanenallee 6, 15735 Zeuthen, Germany
e-mail: rolf.buehler@desy.de

² Institut für Physik, Humboldt-Universität zu Berlin, Newtonstrasse 15, 12489 Berlin, Germany
e-mail: julian.schliwinski@desy.de

Received date / Accepted date

ABSTRACT

Here, we present the IUVA catalog of time variable ultraviolet (UV) sources. We describe a new analysis pipeline, the Variable Source Clustering Analysis (VASCA). We apply the pipeline to 10 years of data from the GALaxy Evolution eXplorer (GALEX) satellite. We analyse a sky area of 302 deg², resulting in the detection of 4202 time-variable UV sources. We cross correlate these sources with multi-frequency data from the *Gaia* satellite and the SIMBAD database, finding an association for 3655 sources. The source sample is dominated by Active Galactic Nuclei ($\approx 73\%$) and stars ($\approx 24\%$). We look at UV and multi-frequency properties of these sources, focusing on the stellar population. We find UV variability for four White Dwarfs. One of them, WD J004917.14-252556.81, has recently been found to be the most massive pulsating White Dwarf. Its Spectral Energy Distribution shows no sign of a stellar companion. The observed flux variability is unexpected and difficult to explain.

Key words. Ultraviolet: general, stars, galaxies – Galaxies: active – Stars: Hertzsprung-Russell and C-M diagrams, white dwarfs

1. Introduction

The study of the time variable sky has historically been a key area in astronomy. The characterization of planet movements and the light emitted by distant supernovae, for example, have fundamentally shaped our understanding of the Universe. More recently, the time variability of stars due to the occultation of orbiting planets, has led to the discovery of thousands of extra-solar planets (Zhu & Dong 2021). Over the past decades, several new classes of variable sources have been found, such as Fast Radio Bursts (Cordes & Chatterjee 2019), Tidal Disruption Events (Gezari 2021), Kilonovae (Abbott et al. 2017) or Pulsar Wind Nebulae (Bühler & Blandford 2014).

Wide field surveys have characterized the time variability of the sky from radio to gamma-ray frequencies (Thyagarajan et al. 2011; Bellm et al. 2019; Lo et al. 2014; Abdollahi et al. 2017). At all wavebands, AGN and/or variable stars make up the bulk of variable sources. The variability observed from stars typically has a thermal photon spectrum, indicating time-variable heating and/or cooling of the star or its environment. For AGN, the variability often shows non-thermal spectra and is therefore linked to acceleration and cooling of cosmic rays. However, exceptions to both of these generalizations exist.

In this article, we study the variability of the UV sky, using data from the GALaxy Evolution eXplorer (GALEX). This satellite scanned $\approx 70\%$ of the sky from 2003 to 2013. To date, its data is still the one with the best UV-coverage in time over a wide field. GALEX took data in two filters, in the NUV ($\lambda_{eff} = 2316 \text{ \AA}$) and FUV ($\lambda_{eff} = 1539 \text{ \AA}$) bands. The FUV sensor failed in 2009, which is why only NUV data is available after this. A summary of the GALEX instrument performance can be found in Morrissey et al. (2007) and a description of its different surveys in Bianchi et al. (2014).

The most detailed systematic characterization of time-variable sources in the GALEX data was done in the Time Domain Survey (TDS, Gezari et al. 2013). The TDS covered an area of 40 deg² finding 1078 UV-variable sources. More recently, a project has been started to create a legacy catalog of GALEX sources using all available GALEX data¹. This catalog shall also include time variability information. As a first result, a catalog of 1426 sources which vary on small time scales of $\lesssim 1500$ sec was derived (Million et al. 2023). Future missions, as ULTRA-SAT (Shvartzvald et al. 2023), the CSST (Zhan 2018) and the proposed UVEX (Kulkarni et al. 2021) are expected to improve the sensitivity of such studies in the coming decade.

In this work, we created the IUVA catalog of variable sources from the GALEX data, extending the sky coverage of the TDS by a factor $\gtrsim 7$. For this, we implemented a new analysis pipeline, the Variable Source Cluster Analysis (VASCA). The article is structured as follows: In section 2, we describe the VASCA pipeline, the GALEX dataset and the source association procedures. In section 3, we present the obtained results and discuss the source classes, focusing on UV variable stars and White Dwarfs (WDs). Finally, we summarize our findings in section 4.

The VASCA code is publicly available on GitHub² and the data products of the IUVA catalog will be made available at the Strasbourg astronomical Data Center (CDS). Throughout this paper we will report spectral flux density in micro Jansky, AB magnitudes will also be given in parallel for comparison with other works.

¹ https://www.millionconcepts.com/documents/glcat_adap_trimmed.pdf

² <https://github.com/rbuehler/vasca>

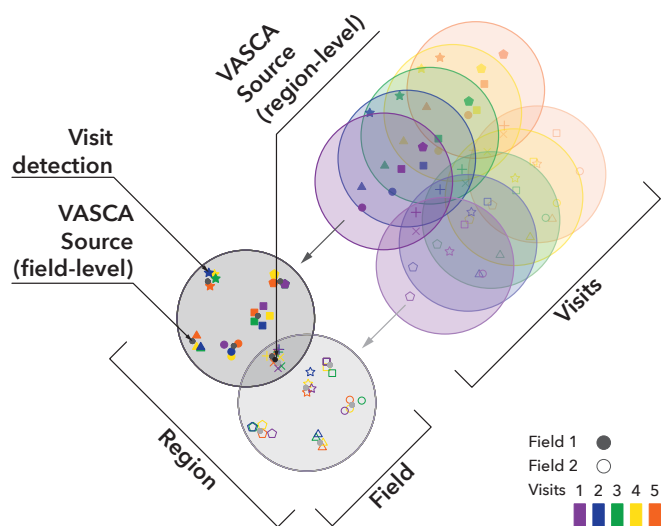


Fig. 1. The VASCA data model, see main text for more details.

2. Variable Source Cluster Analysis pipeline

VASCA offers a modular and scalable analysis pipeline for creating catalogs of cosmic variables from repeated photometric observations. The pipeline is implemented in an instrument independent way. We will describe it using the GALEX data set as a hands-on application in the following.

2.1. Data model and GALEX data set

VASCA is based on a data model that describes photometric detections from repeated observations. These are referred to as “visits” hereafter. A set of visits observing the same patch on the sky in the same pass band defines a “field”. A collection of fields defines a “region”, as shown in figure 1. Fields can also be overlapping, as in fact is often the case for instruments that perform surveys and follow-up observations. The data model is kept simple by only defining these three hierarchical data layers. We emphasize that observations in different pass bands and by different instruments are treated as separate fields, even if they observe the same patch of the sky. Fields are only combined on the region-level. This is fundamentally the reason for the pipeline’s scaling ability and instrument independence.

We applied VASCA to 385 NUV-fields and 270 FUV-fields of the GALEX legacy data on the Multimission Archive at STScI (MAST). These were all fields which fulfilled the following conditions: (1) they have been visited ≥ 10 times in the NUV band (2) the average NUV exposure is > 800 sec. We applied our selection on the NUV band only, as FUV-only data were very rarely taken by GALEX. The number of visits in the NUV band for each considered field in the sky is shown in the appendix A. The average number of visits for each field is 26.6 in the NUV and 18.9 in the FUV. The total exposure is 12.5 Msec in the NUV band and 5.9 Msec in the FUV band. This is approximately 7.7 times the exposure of the TDS. The applied selection ensures a rather uniform data set, with an average exposure time per visit of 1220 sec. The average limiting fluxes at a signal to noise of 3 for the typical visit is therefore $f_{NUV} \approx 2.0 \mu\text{Jy}$ and $f_{FUV} \approx 2.2 \mu\text{Jy}$ ($m_{AB}^{NUV} = 23.1$ and $m_{AB}^{FUV} = 23.0$, respectively).

In this work, we used the GALEX Release 6/7 data products. A description of this standard pipeline and calibration can be

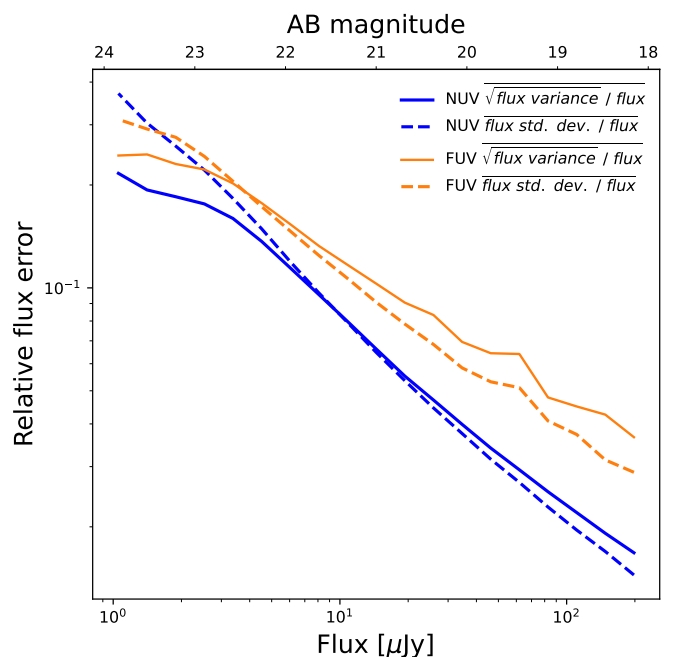


Fig. 2. Comparison of the observed flux variation of VASCA sources, compared to the photometric measurement error, for the NUV (blue lines) and FUV (red lines) pass bands. See text for more details.

found online³ and in Morrissey et al. (2007). Photometry in the NUV and FUV bands are provided in these data products. The systematic flux accuracy of the pipeline photometry is expected to be 0.8% and 2.5% on average for the NUV and FUV bands, respectively.

We cross-checked the accuracy of the photometric measurements by comparing the observed flux variations to the ones expected for the measured flux errors. To avoid the inclusion of strongly variable sources into the data set we only considered sources with a χ^2 -probability to a constant flux $PVAL_{flux} > 0.001$ and more than 5 light-curve points. As can be seen in figure 2, the difference between the observed variations to the ones expected from the measured errors is $< 10\%$ and $< 20\%$ in the NUV and FUV bands, respectively. Under the assumption that the sources are not time variable within the photometric sensitivity of GALEX, this comparison would yield a measure of the GALEX photometry accuracy. However, as low-level variable sources remain in the sample, this corresponds to an upper limit on the stability of the flux determination. These limits are in agreement with the systematic errors quoted previously. Note, that the discrepancy observed at low-flux levels is a selection effect: only upward-flux fluctuations are detected close to the flux sensitivity threshold.

The GALEX images are known to contain several different artifacts, a detailed discussion can be found in Million et al. (2023). These artifacts can potentially create artificial sources or source variability. In order to minimize their effect in our pipeline, we performed stringent quality cuts on the photometric detections. In particular, selection cuts were applied to enforce that only point-like sources are selected, as artifacts are typically extended and asymmetric. Furthermore, we restricted our analysis to the inner camera, where artifacts are more sparse. Finally, we require a minimum of three independent detections for each source, as artifacts typically do not repeat in position over mul-

³ <http://www.galex.caltech.edu/researcher/data.html/>

multiple visits. All selection variables and values are listed in table 1.

2.2. Pipeline and variability selection

A schematic representation of the analysis flow of VASCA is shown in the appendix B. Photometric detections of each visit are inputs to the pipeline. After quality selection, detections are clustered for all visits of each field using the MeanShift algorithm (Pedregosa et al. 2011; Comaniciu & Meer (2002)). The clustering bandwidth is always fixed to $4''$, significantly larger than the typical absolute astrometric performance of $\lesssim 1.5''$ of GALEX (Morrissey et al. 2007).

To handle different observation filters and overlapping fields, a second clustering is performed for all clusters obtained in the field analysis. The clusters obtained in this second step define the position of a 1UVA source. Its position and mean flux are calculated as the error-weighted mean from all detections associated to the individual cluster. For GALEX observations, additional source photometry is typically provided for the sum of all visit images in a field, the so called co-add image. This information is also fed into the pipeline. Co-add image detections are clustered and associated to the sources previously derived from the visit detections.

Statistical measures are calculated to diagnose the source time variability. The primary statistic is the χ^2 -probability for a constant flux. We select sources which are incompatible with a constant flux at a $5\text{-}\sigma$ level. We also select sources which have a significant difference between the mean flux and the co-add flux. The former is defined as the error-weighted mean of the flux in all visit-level detections, while the latter is the one obtained from the photometry of the co-add images. This cut is applied to select sources that are only detected during bright flaring periods in a few visits. All selection values are listed in table 1. To take into account possible systematic flux variations we also select on the normalized excess variance of the flux $NXV_{flux} = (Var_{flux} - err_{flux}^2)/flux^2$, where Var_{flux} and err_{flux} is the variance and error of the flux measurements (Vaughan et al. 2003). The selection on the minimum excess variance corresponds to a flux variability of $\approx 3\%$ and $\approx 10\%$ for the NUV and FUV band, respectively. This is ≈ 4 times the expected photometric stability of GALEX discussed in the previous section, making sure that no instrumental variations lead to artificial variability.

2.3. Source association

In order to find multi-frequency counterparts we check for positional coincidences within $1.5''$ for all 1UVA sources. This match is done with all sources listed in the SIMBAD database (Wenger et al. 2000), the *Gaia*-DR3 and WD catalogs (Gaia Collaboration et al. 2023; Gentile Fusillo et al. 2021) and the recent GALEX Flare Catalog (Million et al. 2023). The latter lists sources which are variable within one visit in GALEX data. If multiple counterparts are found in one catalog, the closest one is preferred.

In order to obtain a Spectral Energy Distribution (SED), we use the VizieR photometry tool⁴. It provides all SED points from all entries in the VizieR database (Ochsenbein et al. 2000). We caution that the latter is done without specific checks on the quality of these catalogs. Finally, we also query if SDSS spectra are available for each source (Abdurro'uf et al. 2022).

⁴ <http://vizier.cds.unistra.fr/vizier/sed/doc/>

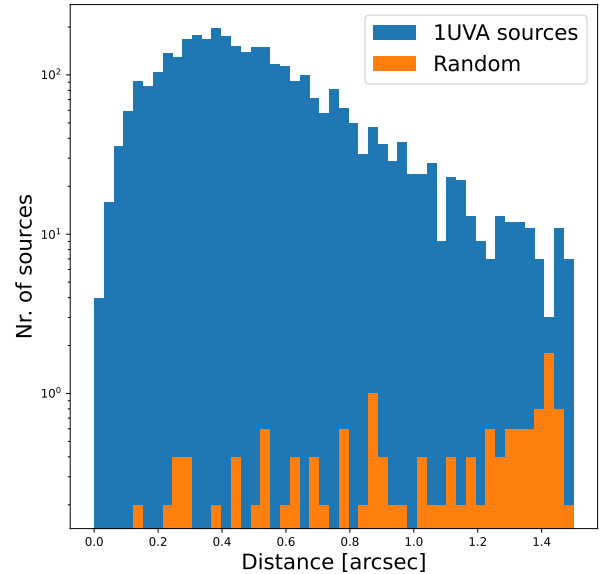


Fig. 3. Angular distance between the 1UVA sources and the associated *Gaia*-DR3 sources, for the measured source positions (blue bars) and randomly scattered positions (orange bars).

2.4. Periodicity search

We performed a periodicity search using a Lomb-Scargle periodogram (Lomb 1976; Scargle 1982) in the frequency range of 0.03 d^{-1} to 2 d^{-1} . For all 1UVA sources we estimate significance of the main peak in the periodograms with the method of Baluev (2008). We include periodicity frequency peaks with a significance greater than $4\text{-}\sigma$ in the catalog, if the light curve contained more than 20 points. We are aware that the usage of these periodicity detections methods has significant caveats in the case of sparse binning, as is typically the case for the light curves in the catalog (for a discussion see e.g. VanderPlas (2018)). We therefore consider the reported periodicities only as tentative. They can be useful to search for periodicity for these sources in the future, with more evenly sampled light curves.

3. Catalog of ultraviolet variable sources

In total, our pipeline found 1991105 UV-sources. Out of these, 4202 sources pass the flux variability selection. The latter compose the 1UVA catalog. A list of the information available for each source in the catalog is provided in appendix C. On average, the light curves of 1UVA sources contain 6.1 photometric measurements in the NUV and 3.4 in the FUV. A wide range of time scales is probed, from ≈ 90 minutes to ≈ 8 years. The distribution of time differences between light-curve points is shown in the appendix A.

We find multi-frequency counterparts for 3656 sources: 3301 sources have a counterpart in the *Gaia*-DR3 catalog and 2686 sources a counterpart in the SIMBAD database. The distance distribution between the 1UVA positions to the associated *Gaia*-DR3 sources is shown in figure 3. The average angular distance is $0.40''$. As the positional uncertainties of *Gaia*-DR3 sources are negligible compared to the ones of GALEX, this also corresponds to the mean positional accuracy of the 1UVA sources.

Table 1. Selection parameters used in the VASCA pipeline.

Variable	Description	Value
<u>Detection quality selection</u>		
S2N	Signal to noise	>3
R_{fov}	Distance to the center of the FoV	<0.5 deg
ELLIP _{world}	Ellipticity	<0.5
SIZE _{world}	Circular extension	<6''
CLASS _{star}	Extended (0) or point like (1)	>0.15
CHKOBJ _{type}	Matched to a bright star (0=no, 1 = yes)	0
APPRATIO _{flux}	Ratio of flux calculated with apertures of 3.8'' and 6.0''	0.3 to 1.05
ARTIFACTS	Detections on-top of variable/hot pixels and of optical reflections are ignored	2, 4, 8, 128 and 256
<u>Variable source selection</u>		
FLUX	Spectral flux density	0.145 μ Jy to 575.4 μ Jy
N_{det}	Number of detections	>3
PVAL _{flux}	Probability of constant flux	< 5.73×10^{-7}
NXV _{flux}	Flux normalized excess variance	>0.001 (>0.01)
FRATIO _{co}	Ratio of the mean flux to the co-add flux	>2
S2N _{co} ^{diff}	Signal to noise of the flux to co-add flux difference	>7
QVAL _{pos}	Cluster position quality parameter	< 5.73×10^{-7}
XV _{pos}	Positional excess variance	<2 arcsec ²

Notes. More details on the detection variables can be found in the GALEX documentation <http://www.galex.caltech.edu/wiki/>. Selection parameters are typically equal for the NUV and FUV bands. If the FUV parameter value differs, it is listed in brackets.

In order to check the chance probability of false associations, we shifted the 1UVA source positions randomly between 2'' and 60'' five times and performed the source association again: on average, only 14.8 *Gaia*-DR3 associations are found, their distance distribution is also shown in figure 3. The low number of random matches confirms the expectation that only few sources are wrongly associated in the catalog. This also confirms that, if at all, only a few spurious sources are part of the 1UVA catalog.

3.1. Source classes

To classify the types of the 1UVA sources, we rely on the classification used in the SIMBAD data base⁵. The distribution of source types is shown in figure 4 and listed in more detail in table 2. Both of them only show SIMBAD counterpart sources with a secured source type.

In general, a large diversity of sources is found. As expected, the vast majority of sources are Active Galactic Nuclei (AGN, $\approx 73\%$). Among these, the subclass of quasars dominated the sample. The second largest class of sources are stars, either single ($\approx 18\%$) or in binary systems ($\approx 5\%$). Non-active Galaxies ($\approx 2.8\%$) and one HII region are also found; these large diffuse objects must have a variable source within them, which is of unknown type at this point.

In two cases, 1UVA sources are associated to a Supernova (SN) explosion. For the first case, 1UVA J141829.9+534331.0, the time profile corresponds to the SN PS1-11pf (Sanders et al. 2015). In the second case, 1UVA J33308.1-271452.5, the observed UV variability precedes the associated "SN cds1 r 20121007 43A" by several years. In addition, the latter is only classified as "Probably Supernova" in the original catalog (Cappellaro et al. 2015). This source is therefore very likely not a SN.

The square root of the flux-excess variance of the different source classes is shown in figure 5, for the NUV and FUV bands. In both bands, the observed variability amplitude varies between

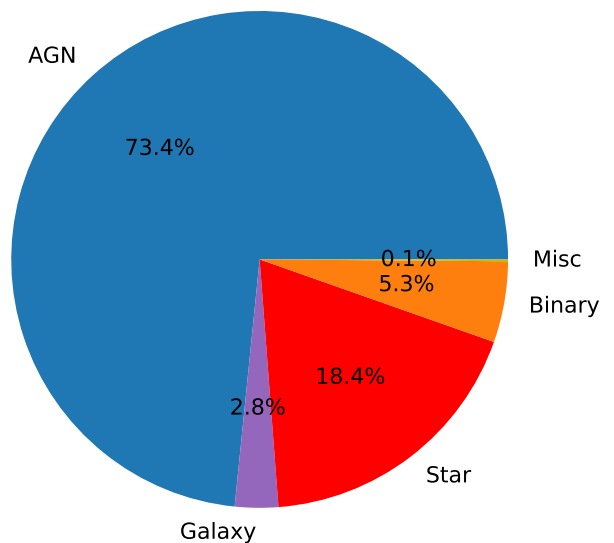


Fig. 4. Object groups for 1UVA counterpart sources with a secured source type in the SIMBAD database. A more detailed subdivision is given in table 2.

a few percent to a factor ≈ 10 . The variability amplitude is generally larger and extends to higher values for stellar objects than for AGN. A similar trend had already been found in the TDS survey (Gezari et al. 2013).

Due to the richness of the data set, a deeper study of all sources types found in the 1UVA catalog is beyond the scope of this article. Here, we will focus on two findings: first, the large variety of different stars that are found in the 1UVA catalog. Second, two WDs are found to be variable, even though their SED

⁵ <http://vizier.u-strasbg.fr/cgi-bin/0Type?§1>

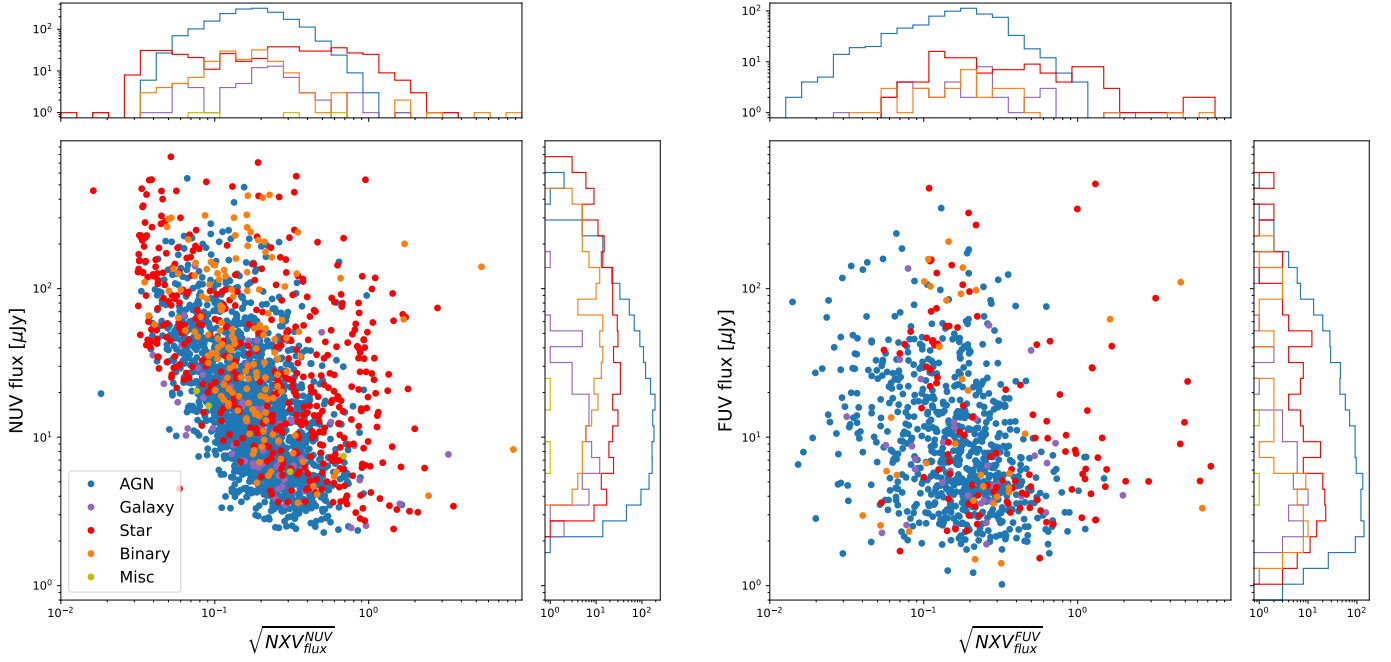


Fig. 5. Flux versus the relative amplitude of flux variations, given by the square root of the normalized excess variance, as a function of the mean flux, for the NUV (left) and FUV (right) pass bands. The axes range is the same in both bands, for an easier comparison. The sub-panels at the top and right of each image show the total number of sources projected onto the respective axis.

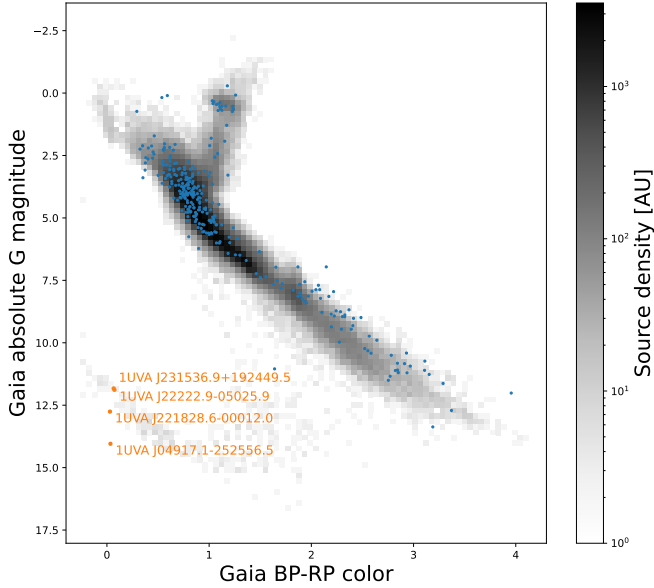


Fig. 6. Hertzsprung-Russell Diagram for VASCA sources with *Gaia*-DR3 counterparts (blue points, see text). The gray background map shows the source density of randomly selected *Gaia*-DR3 sources for comparison. The *Gaia* source selection cuts are the same for both cases. The orange marker shows the UV-variable WDs discussed in section 3.3.

show no sign of any companion star. We will go into more details on both of these findings in the following sections.

3.2. UV-variable stars

As can be seen in table 2, many different stellar classes are found to be UV-variable. The dominant class is RR Lyrae stars, as ex-

pected from previous studies (Gezari et al. 2013). Several other pulsating stars are also found, as Pulsating Variables, Cepheids and delta Sct Variables. Perhaps more surprisingly, 20 High Proper Motion stars are found in the sample.

Using the *Gaia*-DR3 associations, we constructed the Hertzsprung-Russel (HR) diagram of *Gaia* counterparts of 1UVA sources, shown in figure 6. The figure also shows the star density for a random sample of *Gaia* sources. For both, we applied the same quality cuts on the *Gaia* measurements: the signal to noise of the blue and red filter photometry and the parallax measurements all have a signal to noise greater than 10. The fluxes of sources beyond 150 pc are corrected for dust extinction using the estimates from the low-resolution *Gaia* spectra (Andrae et al. 2023). Only sources for which the latter extinction estimate was available were included in the sample. In addition, sources were only included if they have an extinction in the G band $A_G < 1$. Sources closer than 150 pc are all included and not corrected for extinction, as the effect is expected to be small in this case $A_G \lesssim 0.02$.

It is interesting to note that 1UVA sources are found throughout the HR diagram, even though there is strong selection bias towards bluer stars due to the UV selection of the sample. UV variability seems to be ubiquitous for stars, independent whether they are on the main sequence or in the horizontal branch. In the former, a shift towards redder and brighter sources is seen for stars with absolute magnitudes larger than ≈ 7 . This is likely due to the fact that UV variable sources are preferably binary systems (Gaia Collaboration et al. 2018). Finally, WDs stars are also found in the sample.

3.3. UV-variable White Dwarfs

WDs are known to be strongly variable in the ultra-violet when they have a stellar companion. The accretion of matter of the companion star can lead to strong novae explosions in Cataclysmic Variables (CVs) (Inight et al. 2023). Indeed,

Table 2. Types of 1UVA counterparts in the SIMBAD database.

Object group	Type	Description	Nr. sources
AGN	AGN	Active Galaxy Nucleus	87
AGN	BLL	BL Lac	11
AGN	Bla	Blazar	2
AGN	QSO	Quasar	1620
AGN	Sy1	Seyfert 1 Galaxy	127
AGN	Sy2	Seyfert 2 Galaxy	2
AGN	SyG	Seyfert Galaxy	1
AGN	rG	Radio Galaxy	1
Binary	**	Double or Multiple Star	2
Binary	CV*	Cataclysmic Binary	11
Binary	EB*	Eclipsing Binary	109
Binary	No*	Classical Nova	2
Binary	SB*	Spectroscopic Binary	9
Galaxy	BiC	Brightest Galaxy in a Cluster (BCG)	2
Galaxy	EmG	Emission-line galaxy	2
Galaxy	G	Galaxy	62
Galaxy	GiC	Galaxy towards a Cluster of Galaxies	3
Galaxy	GrG	Group of Galaxies	2
Misc	HII	HII Region	1
Misc	SN*	Supernova	2
Star	*	Star	157
Star	AB*	Asymptotic Giant Branch Star	1
Star	BS*	Blue Straggler	1
Star	BY*	BY Dra Variable	1
Star	Em*	Emission-line Star	1
Star	Er*	Eruptive Variable	8
Star	GIC	Globular Cluster	1
Star	HB*	Horizontal Branch Star	5
Star	Ir*	Irregular Variable	2
Star	LM*	Low-mass Star	4
Star	LP*	Long-Period Variable	3
Star	PM*	High Proper Motion Star	20
Star	Pe*	Chemically Peculiar Star	1
Star	Pu*	Pulsating Variable	12
Star	RG*	Red Giant Branch star	2
Star	RR*	RR Lyrae Variable	203
Star	Ro*	Rotating Variable	5
Star	TT*	T Tauri Star	1
Star	V*	Variable Star	22
Star	WD*	White Dwarf	5
Star	WV*	Type II Cepheid Variable	1
Star	Y*O	Young Stellar Object	1
Star	cC*	Classical Cepheid Variable	2
Star	dS*	delta Sct Variable	4
Star	s*b	Blue Supergiant	1

11 CVs counterparts are found for 1UVA sources in the SIMBAD database, see table 2. Time variability has also been found for WDs with sub-stellar companions: the obscuration during eclipses and the heating of the companion can cause flux periodicity on time scales between a few hours and several days (Hernández Santisteban et al. 2016; van Roestel et al. 2021). On short time scales of ≈ 10 min, periodic UV variability has been found for isolated WDs from their rotating photosphere, in so called Pulsators (Rowan et al. 2019).

We searched for isolated variable WDs among the 1UVA sources. For this, we selected sources which have a counterpart that is classified as a WD at $>90\%$ confidence in the *Gaia*-EDR3 WD catalog. Four 1UVA counterpart sources passed this selection, their properties are listed in table 3. Note, that this classi-

fication is more reliable than the one of the SIMBAD database used previously. Indeed, two sources which had been classified as WDs in the SIMBAD database showed a probability $< 35\%$ of being a WD in the *Gaia*-EDR3 WD catalog (1UVA J234829.1-92500.3 and 1UVA J221409.9+05246.0). We therefore did not include them in this discussion.

The SED of these sources is shown in the left panels of figure 7. No companion star is visible in all cases. To emphasize this point, we show the SED of a putative dim brown dwarf star companion in the SED in this figure. The star was assumed to have a radius of $0.1R_{\odot}$ and to have a temperature of 2700K. As one can see, the measured fluxes are about an order of magnitude below the expected stellar emission, particularly in the infrared.

Table 3. Properties of the WDs associated with the sources shown in figure 7.

1UVA ID	J04917.1-252556.5	J221828.6-00012.0	J22222.9-05025.9	J231536.9+192449.5
WD ID	J004917.14-252556.81	J221828.58-000012.17	J022222.85-005026.59	J231536.88+192449.14
Distance	99.6 pc	121.7 pc	371.6 pc	168.9 pc
Spectrum	DA	DAH	DA	Unknown
Temperature	14145 K	11514 K	11831 K	12483 K

Notes. The WD ID refers to the *Gaia*-EDR3 WD catalog and the temperature to the Black Body fit shown in figure 7.

The UV light curve of the four WDs is shown in the right panels of figure 7. All of them are clearly variable. The variability time scale has to be larger than the typical observation time of ≈ 24 min. In several cases, indications of long-term trends of time scales of days to years are apparent: e.g. for WD J004917.14-252556.81 all fluxes measured in 2009 are below the ones measured in 2004. However, due to the scarcity of the data, it is possible that these trends are in fact due to the random sampling of shorter term variability.

One of the sources, WD J221828.58-000012.17, is classified as a magnetic WD. Flux variations from magnetic WDs are well known (Lawrie et al. 2013): they are related to the rotation of the WD and have a period between several minutes to several days. The typical peak-to-peak amplitude of the flux variations are a few percent. Even so no periodicity can be measured in the UV data due to its scarcity, this might explain the observed flux variations for this source.

Two sources, WD J004917.14-252556.81 and WD J022222.85-005026.59, are classified as normal DA WDs. Variability time scales ≥ 24 min is not usual for these sources. It might hint at an ongoing accretion from an undetected substellar companion. However, no companion was seen in the SED and no spectral lines from an accretion disk can be seen in the optical to infrared spectrum (Kilic et al. 2023b). Another possibility is that planetary debris is absorbing the light from the WD periodically (Vanderbosch et al. 2020). A third possibility might be that the temperature of the photosphere is changing due to a yet unknown reason.

Particularly interesting is the WD J004917.14-252556.81, as pulsations with a period of $T_{P1} = 221.36$ sec and $T_{P2} = 209.3$ sec have been found from this source (Kilic et al. 2023a). The peak-to-peak amplitude of the pulsations is $\approx 30\%$. This source is the most massive WD from which pulsations have been found to date. We looked for these periodic signals in GALEX data: we derived a light curve sampled in 40 sec bins using the gPhoton tool (Million et al. 2016). We found this to be the smallest time binning at which the photon count rate per bin is still acceptable. Note, that this time binning does unfortunately not allow to resolve the periods T_{P1} and T_{P2} separately.

As the WD oscillations might drift with time (Kilic et al. 2023a), we searched for periodicity's running a Lomb Scargle test for the four observing blocks in the GALEX data: MJD 52925.31975–52925.61277, 55096.10218–55097.06439, 55104.57558–55106.78567 and 55123.12991–55128.62543. The periodogram is shown in the appendix D. No significant pulsations were found in all except the third observing block. During this observing block a peak is found in the periodogram at $T_P = \approx 218$ sec with a false probability of 0.10%. This period is in agreement with T_{P1} and T_{P2} within the accuracy of the time binning of our data. We therefore consider this an indication that the found oscillations are also present in the UV, at least during some time periods. More sensitive UV observations with a finer time resolution will be needed to settle this question.

4. Summary and Outlook

We have presented the 1UVA source catalog of variable UV sources. We described a novel analysis pipeline, called VASCA, to cluster and diagnose sources found in photometric data. We applied the VASCA pipeline to GALEX data, finding 4202 variable UV-sources that vary in time scales between ≈ 30 min to several years. We found a multi-frequency counterpart for 3655 of these sources. As expected, AGN dominate the source sample by numbers. The second largest group are variable stars.

We found, that UV-variability is ubiquitous for stellar objects, even for those which are not in binary systems; UV-variable stars are found in all regions of the HR diagram. We then focused our attention on WDs, which are not in CV systems, finding four variable WDs. One of them, WD J004917.14-252556.81, is particularly interesting. This source has recently been found to be the most massive WD with seismic periodic oscillations (Kilic et al. 2023a). We found indications for these pulsations also in the GALEX UV data. The observed UV variability from this source is puzzling and we speculated on several possible scenarios.

Due to its modularity and instrument independence, VASCA can be applied to different surveys in the future. The only requirement is that photometric measurements are available on a visit level, before co-adding the data. Such data is for instance expected to be available for the upcoming ULTRASAT mission (Shvartzvald et al. 2023), *Vera Rubin* telescope (Ivezic et al. 2019) and Cherenkov Telescope Array (Actis et al. 2011) data. For future UV data, the 1UVA catalog provides a long time baseline, that can be used to study UV flux variability over several decades.

Finally, we want to mention that due to richness of the 1UVA dataset, we could only focus our attention on selected sources in this work. We encourage the usage of the VASCA code and the catalog data products for further studies.

Acknowledgements. We thank Thomas Kupfer for insightful discussion on the presented work. This work made use of Astropy (Astropy Collaboration et al. 2022), scikit-learn (Pedregosa et al. 2011), the SIMBAD database (Wenger et al. 2000) and the VizieR catalogue access tool (DOI : 10.26093/cds/vizier).

References

- Abbott, B. P., Abbott, R., Abbott, T. D., et al. 2017, *ApJ*, 848, L12
 Abdollahi, S., Ackermann, M., Ajello, M., et al. 2017, *ApJ*, 846, 34
 Abdurro'uf, Accetta, K., Aerts, C., et al. 2022, *ApJS*, 259, 35
 Actis, M., Agnetta, G., Aharonian, F., et al. 2011, *Experimental Astronomy*, 32, 193
 Andrae, R., Fouesneau, M., Sordo, R., et al. 2023, *A&A*, 674, A27
 Astropy Collaboration, Price-Whelan, A. M., Lim, P. L., et al. 2022, *ApJ*, 935, 167
 Baluev, R. V. 2008, *MNRAS*, 385, 1279
 Bellm, E. C., Kulkarni, S. R., Graham, M. J., et al. 2019, *PASP*, 131, 018002
 Bianchi, L., Conti, A., & Shiao, B. 2014, *Advances in Space Research*, 53, 900
 Bühler, R. & Blandford, R. 2014, *Reports on Progress in Physics*, 77, 066901
 Cappellaro, E., Botticella, M. T., Pignata, G., et al. 2015, *A&A*, 584, A62

- Comaniciu, D. & Meer, P. 2002, IEEE Transactions on Pattern Analysis and Machine Intelligence, 24, 603
- Cordes, J. M. & Chatterjee, S. 2019, ARA&A, 57, 417
- Gaia Collaboration, Babusiaux, C., van Leeuwen, F., et al. 2018, A&A, 616, A10
- Gaia Collaboration, Vallenari, A., Brown, A. G. A., et al. 2023, A&A, 674, A1
- Gentile Fusillo, N. P., Tremblay, P. E., Cukanovaite, E., et al. 2021, MNRAS, 508, 3877
- Gezari, S. 2021, ARA&A, 59, 21
- Gezari, S., Martin, D. C., Forster, K., et al. 2013, ApJ, 766, 60
- Hernández Santisteban, J. V., Knigge, C., Littlefair, S. P., et al. 2016, Nature, 533, 366
- Inight, K., Gänsicke, B. T., Breedt, E., et al. 2023, MNRAS, 524, 4867
- Ivezić, Ž., Kahn, S. M., Tyson, J. A., et al. 2019, ApJ, 873, 111
- Kilic, M., Córscico, A. H., Moss, A. G., et al. 2023a, MNRAS, 522, 2181
- Kilic, M., Moss, A. G., Kosakowski, A., et al. 2023b, MNRAS, 518, 2341
- Kulkarni, S. R., Harrison, F. A., Grefenstette, B. W., et al. 2021, arXiv e-prints, arXiv:2111.15608
- Lawrie, K. A., Burleigh, M. R., Brinkworth, C. S., et al. 2013, in Astronomical Society of the Pacific Conference Series, Vol. 469, 18th European White Dwarf Workshop., ed. J. Krziesiński, G. Stachowski, P. Moskalik, & K. Bajan, 429
- Lo, K. K., Farrell, S., Murphy, T., & Gaensler, B. M. 2014, ApJ, 786, 20
- Lomb, N. R. 1976, Ap&SS, 39, 447
- Million, C., Fleming, S. W., Shiao, B., et al. 2016, ApJ, 833, 292
- Million, C. C., Clair, M. S., Fleming, S. W., Bianchi, L., & Osten, R. 2023, ApJS, 268, 41
- Morrissey, P., Conrow, T., Barlow, T. A., et al. 2007, ApJS, 173, 682
- Ochsenbein, F., Bauer, P., & Marcout, J. 2000, A&AS, 143, 23
- Pedregosa, F., Varoquaux, G., Gramfort, A., et al. 2011, Journal of Machine Learning Research, 12, 2825
- Rowan, D. M., Tucker, M. A., Shappee, B. J., & Hermes, J. J. 2019, MNRAS, 486, 4574
- Sanders, N. E., Soderberg, A. M., Gezari, S., et al. 2015, ApJ, 799, 208
- Scargle, J. D. 1982, ApJ, 263, 835
- Shvartzvald, Y., Waxman, E., Gal-Yam, A., et al. 2023, arXiv e-prints, arXiv:2304.14482
- Thyagarajan, N., Helfand, D. J., White, R. L., & Becker, R. H. 2011, ApJ, 742, 49
- van Roestel, J., Kupfer, T., Bell, K. J., et al. 2021, ApJ, 919, L26
- Vanderbosch, Z., Hermes, J. J., Dennihy, E., et al. 2020, ApJ, 897, 171
- VanderPlas, J. T. 2018, ApJS, 236, 16
- Vaughan, S., Edelson, R., Warwick, R. S., & Uttley, P. 2003, MNRAS, 345, 1271
- Wenger, M., Ochsenbein, F., Egret, D., et al. 2000, A&AS, 143, 9
- Zhan, H. 2018, in 42nd COSPAR Scientific Assembly, Vol. 42, E1.16–4–18
- Zhu, W. & Dong, S. 2021, ARA&A, 59, 291

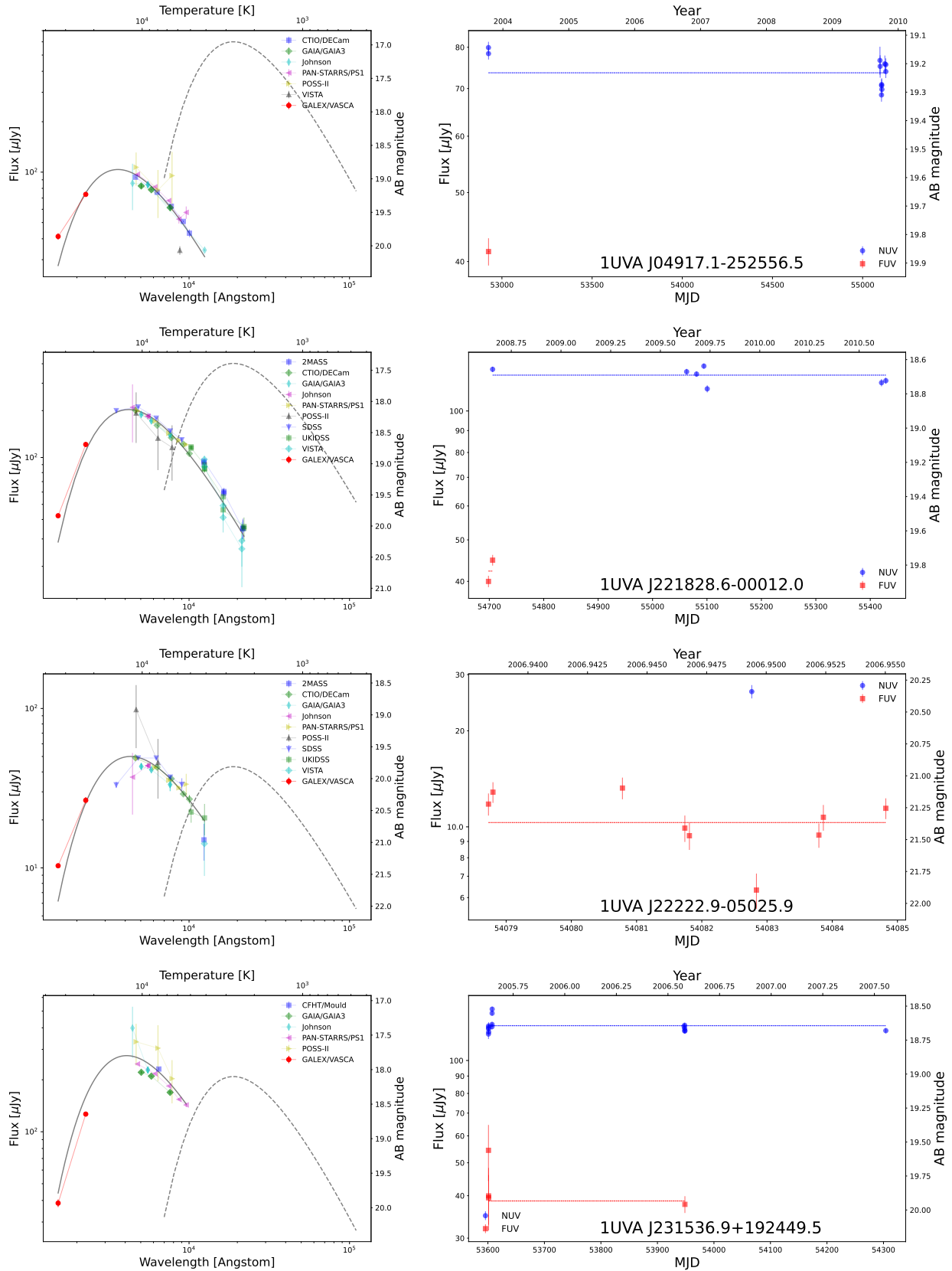


Fig. 7. SED (left) and light curve (right) for the sources listed in table 3. **Left:** The straight line shows the best fit to a black body emission spectrum. The black body temperature is listed in table 3. The dashed line shows the SED of a brown dwarf star in a black body approximation (see main text). **Right:** The dashed line shows the mean flux value.

Appendix A: GALEX observations

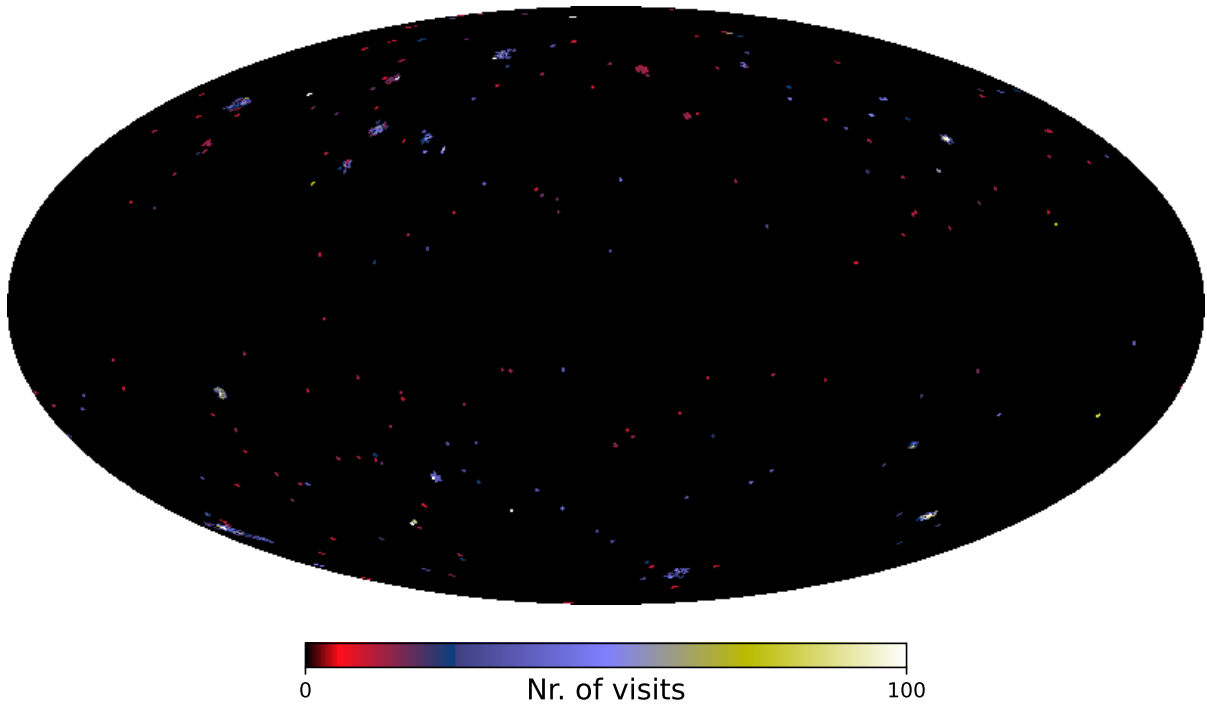


Fig. A.1. Number of visits with NUV exposure for each field considered in the IUVA catalog. The sky map is shown in galactic coordinates in a Mollweide projection.

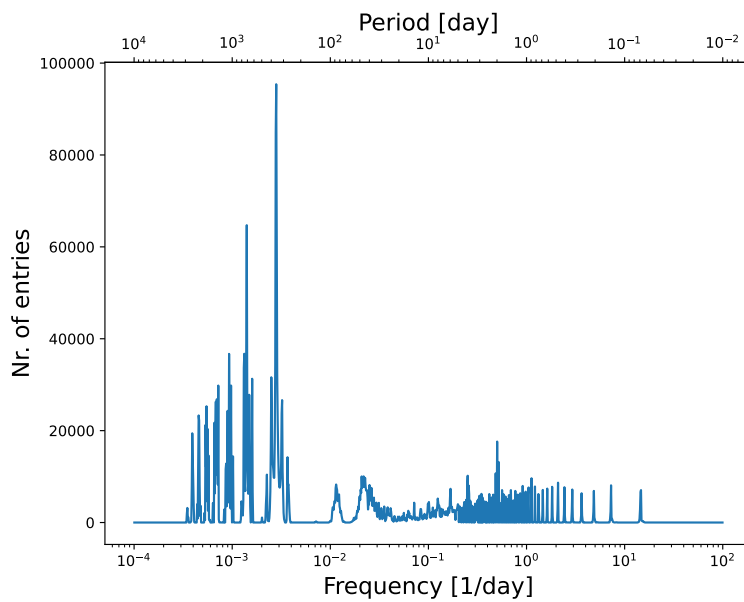


Fig. A.2. Time difference distribution between all combinations of light-curve points for the IUVA sources.

Appendix B: VASCA processing flow

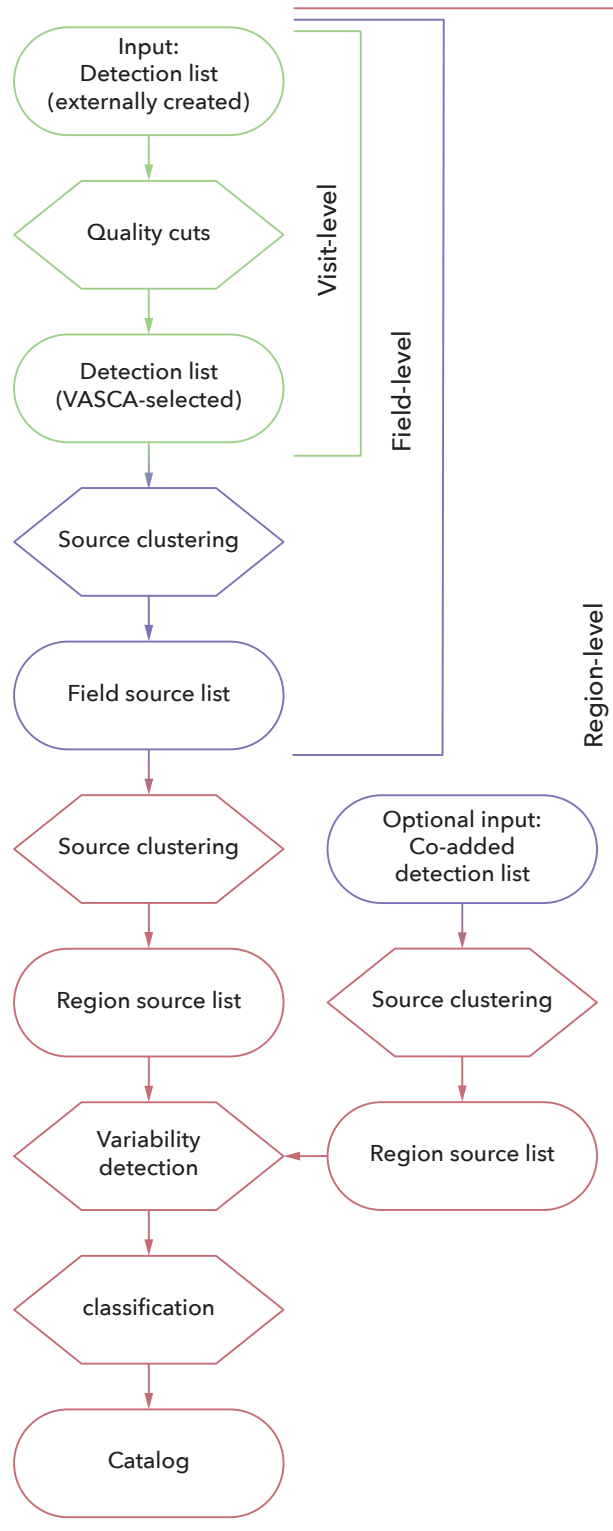


Fig. B.1. Schematic of the VASCA processing flow.

Appendix C: Catalog tables content

Table C.1. Columns of the “SOURCES” table of the IUVA catalog.

Name	Description	Unit
SRC_NAME	VASCA catalog source name	
NR_DET	Number of detections	
RA	Sky coordinate Right Ascension (J2000)	degree
DEC	Sky coordinate Declination (J2000)	degree
POS_ERR	Sky coordinate position error	arcsec
POS_XV	Sky position excess variance	arcsec ²
POS_VAR	Sky position variance	arcsec ²
POS_CPVAL	Sky position quality	
POS_RCHIQ	Sky position reduced chisquared of the constant mean	
FLUX	Flux density	μJy
FLUX_ERR	Flux density error	μJy
FLUX_NXV	Flux normalized excess variance	
FLUX_VAR	Flux variance	10^{-12}Jy^2
FLUX_CPVAL	Probability value for a constant flux from the chisquare test	
FLUX_RCHIQ	Flux reduced chisquared of the constant mean	
COADD_SRC_ID	Co-add source ID number	
COADD_FFACTOR	Source flux divided by flux of the associated co-add source	
COADD_FDIFF_S2N	Signal to noise of the flux difference	
RG_SRC_ID	Region source ID number	
NR_FD_SRCS	Number of field sources	
HR	Flux hardness ratio, only simultaneous detections considered	
HR_ERR	Flux hardness ratio error	
OGRP_SIMBAD	SIMBAD source type group in VASCA	
OTYPE_SIMBAD	SIMBAD source type	
MAIN_ID_SIMBAD	SIMBAD main ID	
SOURCE_GAIADR3	<i>Gaia</i> DR3 source ID	
WDJNAME_GAIAEDR3_WD	<i>Gaia</i> -EDR3-WD object name	
OBJID_GFCAT	GFCAT object ID	
LS_PEAK_PVAL	LombScargle power probability value	
LS_PEAK_FREQ	LombScargle peak frequency	d^{-1}

Table C.2. Tables of the IUVA catalog.

Name	Description
SOURCES	Properties of the IUVA sources
DETECTIONS	Properties of detections of IUVA sources
FIELDS	Properties of the analysed fields
VISITS	Properties of the analysed visits
FILTERS	Observation filter description
COADD_SOURCES	Properties of the co-add sources

Appendix D: Periodogram of White Dwarf J004917.14-252556.81

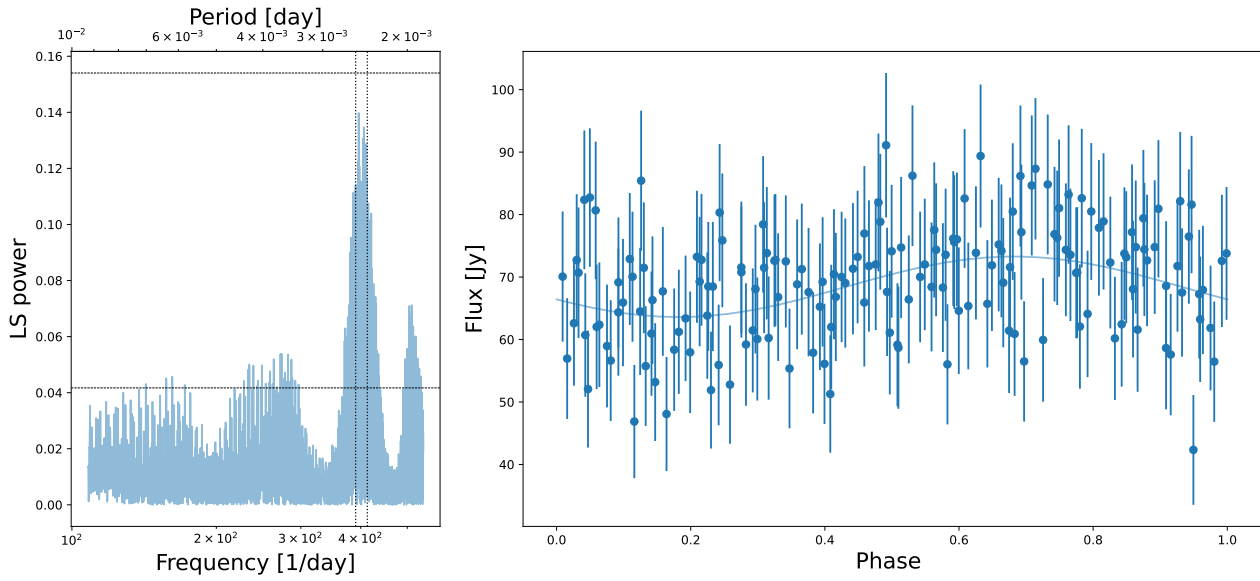


Fig. D.1. **Left:** Lomb Scargle periodogram of the source 1UVA J04917.1-252556.5. It was calculated from a UV light curve in a 40 second time binning, restricted to the time range between MJD 55104.57558–55106.78567. Dashed horizontal lines mark the 2 and 3 σ confidence level calculated following Baluev (2008). Vertical dotted lines mark the periods previously found for this source (Kilic et al. 2023a). For more information see the main text. **Right:** The phased light curve with the best-fit model (straight line).